

# Tunable Mott Dirac and Kagome Bands Engineered on 1T-TaS<sub>2</sub>

Dongheon Lee, Kyung-Hwan Jin,\* Feng Liu, and Han Woong Yeom\*



Cite This: *Nano Lett.* 2022, 22, 7902–7909



Read Online

ACCESS |

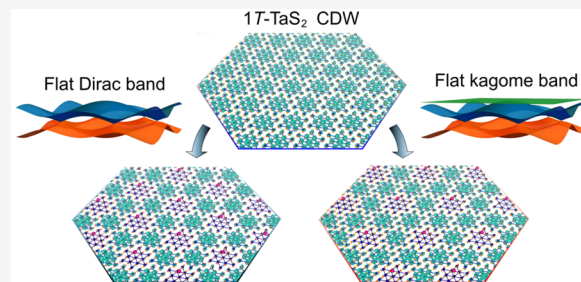
Metrics & More

Article Recommendations

Supporting Information

**ABSTRACT:** Strongly interacting electrons in hexagonal and kagome lattices exhibit rich phase diagrams of exotic quantum states, including superconductivity and correlated topological orders. However, material realizations of these electronic states have been scarce in nature or by design. Here, we theoretically propose an approach to realize artificial lattices by metal adsorption on a 2D Mott insulator 1T-TaS<sub>2</sub>. Alkali, alkaline-earth, and group 13 metal atoms are deposited in ( $\sqrt{3} \times \sqrt{3}$ ) R30° and 2 × 2 TaS<sub>2</sub> superstructures of honeycomb- and kagome-lattice symmetries exhibiting Dirac and kagome bands, respectively. The strong electron correlation of 1T-TaS<sub>2</sub> drives the honeycomb and kagome systems into correlated topological phases described by Kane-Mele-Hubbard and kagome-Hubbard models. We further show that the 2/3 or 3/4 band filling of Mott Dirac and flat bands can be achieved with a proper concentration of Mg adsorbates. Our proposal may be readily implemented in experiments, offering an attractive condensed-matter platform to exploit the interplay of correlated topological order and superconductivity.

**KEYWORDS:** flat band, 1T tantalum disulfide, chemical decoration, artificial lattice



Artificial two-dimensional (2D) lattice systems have been a field of research for the last two decades because they not only reveal the rich fundamental physics of 2D systems but also promise applications in novel quantum devices.<sup>1</sup> Interesting examples include the nanopatterned semiconductor 2D electron gas,<sup>2–6</sup> trapped cold atoms in optical lattices,<sup>7–9</sup> and confined photonic crystals,<sup>10–12</sup> to name just a few. In particular, artificial 2D quantum materials with topological bands originating from the honeycomb lattice symmetry have been successfully realized by the manipulation of CO molecules on a metallic surface<sup>2</sup> (molecular graphene of Dirac bands) and self-assembled deposition of Bi atoms deposited on a patterned semiconductor surface<sup>13–16</sup> (bismuthene, atomic graphene with large spin-orbit coupling to open a gap at the Dirac point). These systems exhibit “man-made” Dirac Fermions and large-gap topological insulating states, respectively.

While the above examples deal primarily with *single-particle* physics, novel artificial 2D electronic lattices may be realized with an inherently strong electron correlation. Namely, one may start with a correlated electronic system of a narrow bandwidth (“flat bands” with  $\sim k^0$  dispersion)<sup>17</sup> and strong on-site Coulomb interaction as a platform to build an artificial lattice. If successful, this approach would offer a chance to engineer and explore novel topological states within the context of *many-body* physics. In this context, we note the superstructure of potassium adatoms on the triangular lattice of 2D Mott insulator 1T-TaS<sub>2</sub>, which was reported to induce effectively an artificial honeycomb lattice Mott insulator.<sup>17</sup> This type of system has significant merit in creating novel

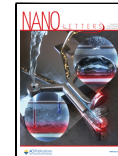
electronic systems with strong interactions. First, it is a 2D solid-state Mott lattice, where strong electron-electron interaction is inherently present,<sup>18–23</sup> so that various exotic quantum phases, such as nontrivial topological states,<sup>17,24–26</sup> quantum spin liquids,<sup>27</sup> unconventional superconductivity,<sup>28,29</sup> and fractional excitations,<sup>30</sup> can be accessed. Second, as a surface- and thin-film-based system, the correlated electronic states can be directly probed by surface techniques, such as scanning tunneling microscopy. Third, it may offer controllability over correlated Fermions via the adsorption of different elements on its surface.<sup>17,31–33</sup>

In the present work, we exploit such merits of adsorbate superstructures on the 1T-TaS<sub>2</sub> Mott insulator using density functional theory (DFT) calculations. We investigate different superstructures of alkali, alkaline-earth, and group 13 metal adatoms on single layer 1T-TaS<sub>2</sub> and propose a practical scheme to fabricate tunable artificial hexagonal and kagome lattices of Mott insulators. Dirac and kagome bands with extremely narrow band widths can be created by metal adatoms in ( $\sqrt{3} \times \sqrt{3}$ ) R30° and 2 × 2 superstructures on a single layer of 1T-TaS<sub>2</sub>, respectively. The alkali and group 13 elements, transferring one electron to the adsorption site, form hexagonal or kagome bands with a Mott gap; while the

Received: July 21, 2022

Revised: September 23, 2022

Published: September 26, 2022



alkaline-earth elements, donating two electrons to the TaS<sub>2</sub> layer, induce 2/3- or 3/4-filled Mott phases. These results demonstrate the possibility of fabricating topological lattices of specific correlated electronic systems and manipulating them via selective atomic adsorption.

## ■ ENGINEERED 2D MOTT HEXAGONAL- AND KAGOME-LATTICE BANDS

We begin with a simple triangular lattice of a single-orbital basis with a nearest-neighbor hopping integral  $t$  to describe the band structure in 1T-TaS<sub>2</sub> in its well-established charge density wave (CDW) state.<sup>17,34</sup> In this minimal model, the tight-binding (TB) Hamiltonian is written as

$$H = -t \sum_{\langle i,j \rangle} (c_i^\dagger c_j + H.c.) - \delta\mu \sum_i c_i^\dagger c_i \quad (1)$$

where  $c_i^\dagger$  and  $c_j$  are the electron creation and annihilation operators at sites  $i$  and  $j$ , respectively. The second term represents the on-site energy shift  $\delta\mu$  due to the potential variation of the adatom at adsorbed site  $i$ . In the case of a half-filled system in 1T-TaS<sub>2</sub>, the on-site energy of the flat band can be easily changed by the direct electron transfer from adatoms.<sup>17,32</sup> There are two key points of interest to be noted. First, the parent triangular lattice of the CDW state [the star of David (DS) distortion] of 1T-TaS<sub>2</sub> can be effectively patterned by altering the on-site potentials ( $\delta\mu$ ) and be turned into hexagonal (Figure 1a) and kagome (Figure 1b) superlattice hosting Dirac (Figure 1c, right panel) and kagome bands (Figure 1d, right panel), respectively. Second, because of minimal hopping ( $t \ll 1$ ), the bands have a very narrow width ( $\leq 0.02$  eV), which we refer to as “flat bands”. They should be distinguished from the single flat band arising from a kagome lattice due to destructive interference, which is inherently flat independent of the magnitude of hopping parameter  $t$ .<sup>35</sup> However, in terms of highly quenched electron kinetic energy and hence significantly enhanced electron–electron interaction, which is of our interest here, the effect of flatness is similar.

Specifically, as shown in Figures 1a and 1b, one converts the triangular lattice into a hexagonal (or kagome) lattice by shifting the on-site energy of one DS among the three (or four) DSs in the supercell. The resulting bands are shown in Figures 1c and 1d. When the on-site energy perturbation is turned off, the narrow parabolic bands are simply folded into the Brillouin zone of the given supercell, as shown in the left panels of Figures 1c and 1d. With the periodic on-site perturbation in a  $(\sqrt{3} \times \sqrt{3})R30^\circ$  supercell, the Dirac state at the K point emerges, resembling that of graphene (Figure 1c); while the kagome lattice can be realized by introducing the on-site potential at one lattice site within a  $2 \times 2$  supercell of the triangular lattice, as evidenced by the typical kagome bands<sup>35</sup> shown in Figure 1d resulting from the remaining unperturbed three sites. All three bands have a very narrow width since the hopping to neighboring sites is limited, which are considered generally as flat bands here, although the top band would be inherently flat even with a large  $t$ . As a result of their flatness, a moderate electron correlation  $U$  will induce a Mott gap, and the newly engineered flat Dirac and kagome bands will become Mott states.

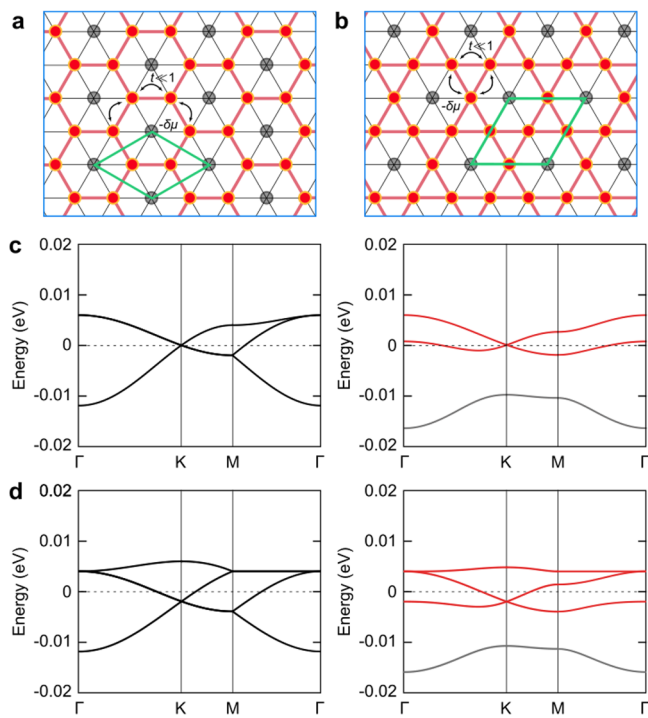


**Figure 1.** An effective model of engineered 2D flat bands. Schematics illustrating an engineered (a) hexagonal lattice and (b) kagome lattice from a trigonal lattice with a very small hopping integral ( $t \ll 1$ ). Each circle indicates a CDW cluster, such as the star of David in 1T-TaS<sub>2</sub>. Atomically perturbed sites (on-site potential shifted by  $-\delta\mu$ ) and unperturbed sites are represented by gray and red colors, respectively. (c) Band structure in a  $(\sqrt{3} \times \sqrt{3})R30^\circ$  supercell without and with on-site energy perturbation  $\delta\mu$ , respectively. The TB hopping parameters used are  $t = 0.002$  eV and  $\delta\mu = 0.01$  eV. (d) Band structure in a  $2 \times 2$  supercell without and with on-site energy perturbation  $\delta\mu$ , respectively. The TB parameters used are the same as in (c). The states contributed from perturbed (unperturbed) sites are indicated by gray (red) color.

## ■ REALISTIC MATERIAL SYSTEM: METAL ADATOMS ON TAS<sub>2</sub> CDW

The theoretical model of a correlated topological lattice we proposed above can be readily realized in a real material platform based on an approach of patterning the localized Mott electrons on the TaS<sub>2</sub> surface. First, we have theoretically investigated the adsorption properties of alkali (Li, Na, K, and Rb), alkaline-earth (Mg, Ca, and Sr), and group 13 (Al, Ga, In, and Tl) metal adatoms on 1T-TaS<sub>2</sub>. For the computational details,<sup>36–41</sup> see the Supporting Information. As described in the TB model, the metal adatoms act as a local perturbation to tune the on-site potential, so as to turn the parent triangle lattice into a hexagonal or kagome superlattice, and hence the band structure, while at the same time donating electrons to shift the Fermi level. Figures 2a and 2b show the  $(\sqrt{3} \times \sqrt{3})R30^\circ$  and  $2 \times 2$  supercells corresponding to a hexagonal and kagome lattice symmetry, respectively. The metal adatom is adsorbed within one of three (or four) DSs in the supercell. To find the most stable adsorption site for the metal adatom, we have evaluated the binding energies for seven candidate hollow sites shown in Figure 2c. We define the binding energy ( $E_b$ ) as

$$E_b = E_{M/TaS_2} - E_{TaS_2} - E_M \quad (2)$$

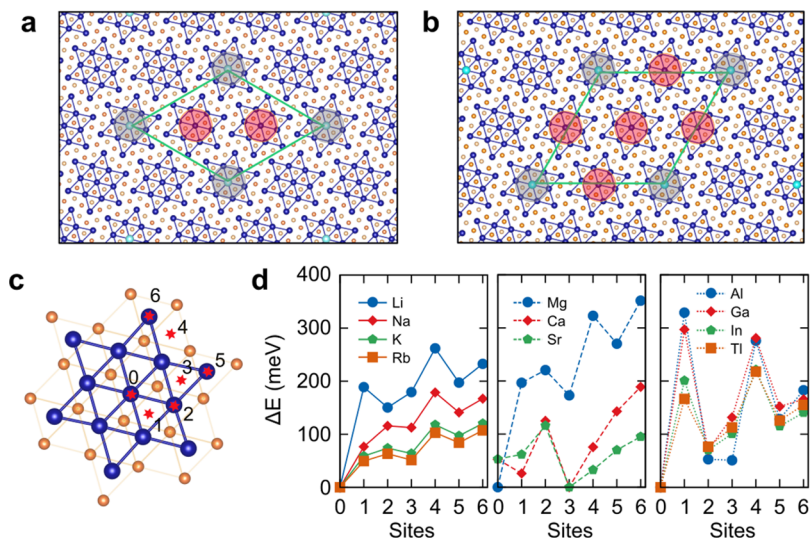


**Figure 2.** Metal adatoms on 1T-TaS<sub>2</sub> CDW. Adatom at the DS center site in periodic (a) ( $\sqrt{3} \times \sqrt{3}$ )R30° and (b) 2 × 2 arrangements on a 1T-TaS<sub>2</sub> monolayer, respectively. The metal adsorbed (bare) DS site is indicated by gray (red) circles. (c) The seven adsorption sites are considered. Only the first two layers of TaS<sub>2</sub> are plotted for clarity. (d) The relative adsorption energies ( $\Delta E$ ) are in reference to that of the lowest-energy site for alkali metal (Li, Na, K, and Rb), alkaline-earth metal (Mg, Ca, and Sr), and group 13 metal (Al, Ga, In, and Tl) elements.

where  $E_{M/\text{TaS}_2}$  is the total energy of the metal adatom on TaS<sub>2</sub>,  $E_{\text{TaS}_2}$  is the total energy of TaS<sub>2</sub> without the metal adatom, and  $E_M$  is the total energy of an isolated metal atom. The relative binding energies for all sites are plotted in Figure 2d in reference to the energy of the most stable site. For alkali and group 13 metals, the most stable site is the center of the DS, labeled as 0, while the off-center site, labeled as 3, is favored by alkaline-earth metals except Mg. Only the 0- or 3-sites are found stable for the adatoms from our calculations. The energy difference between different sites and the height of the adatom ( $h$ ) both decrease with the adatom size in the same group. The height of the adatom is defined as the difference in the  $z$  coordinate of the adatom and the average of the  $z$  coordinates of the top S atoms in the TaS<sub>2</sub> layer (Table 1). For the adatoms we choose, the relatively high ratios of adsorption energy to bulk cohesive energy suggest that they prefer to form 2D layers on the TaS<sub>2</sub> surface, as opposed to 3D clusters, in

agreement with experiments.<sup>17,32</sup> One notes that some defects or charge doping can cause the collapse of the CDW order of 1T-TaS<sub>2</sub> bulk,<sup>42–45</sup> but differently, our approach is based on an ordered superstructure of metals on the surface. Also, the bonding character of metal adsorption is ionic, the structural distortion of DS induced by adatoms is insignificant, and the overall DS structure is maintained (Figure S1).

In order to reveal the electronic interaction between adatoms and the substrate, we estimate the charge state of adatoms using the Bader charge analysis.<sup>46</sup> We found that 0.6–1.0 electrons are transferred from alkali and group 13 metals to the TaS<sub>2</sub> surface. That means their charge states correspond to +1. On the other hand, alkaline-earth metals donate 1.3–1.5 electrons to the TaS<sub>2</sub> surface, which is considered as a +2 charge state. This difference is easily expected and has a profound effect on the band structures, which will be discussed below. On the other hand, while the group 13 metals tend to fall into the +3 oxidation state in bulk compounds, the +1 charge state is favored in the present system. The valence  $p$  states of Al, Ga, and In adatoms are positioned above the Fermi level, while the valence  $s$  state is fully occupied. That is, a group 13 adatom behaves chemically like an alkali adatom with only one of its  $p$  electrons transferred to the surface. Similar behavior was observed on graphene.<sup>47</sup>

## ■ HALF-FILLED MOTT INSULATOR: NA DECORATED TAS<sub>2</sub> SYSTEM

With the adsorption behavior of individual adatoms established above, we first focus on the electronic band structures of hexagonal and kagome lattices formed by Na adatom, as a representative case of the adatom doping one electron to the TaS<sub>2</sub> (See Figures S2 and S3 for results of other adatoms.). Figures 3a–3d show the band structures and the charge density distributions of Hubbard bands for 1T-TaS<sub>2</sub> with Na adatoms in a ( $\sqrt{3} \times \sqrt{3}$ )R30° superstructure. The pristine CDW phase of 1T-TaS<sub>2</sub> generates one narrow half-filled band with an unpaired 5d Ta electron in each unit cell.<sup>20</sup> Therefore, there are three narrow bands involved in the ( $\sqrt{3} \times \sqrt{3}$ )R30° hexagonal superlattice, one of which is fully occupied by one

**Table 1. Metal Adsorption Properties of 1T-TaS<sub>2</sub><sup>a</sup>**

atom	site	$E_b$ (eV)	$E_c$ (eV)	$ E_b /E_c$	$h$ (Å)	$\Delta e$
Li	0	-3.07	1.63	1.88	1.66	0.86
Na	0	-2.49	1.113	2.24	2.23	0.85
K	0	-2.79	0.934	2.99	2.76	0.88
Rb	0	-2.81	0.852	3.30	2.95	0.89
Mg	0	-1.61	1.51	1.07	1.78	1.33
Ca	3	-3.51	1.84	1.91	2.06	1.46
Sr	3	-3.43	1.72	2.00	2.29	1.52
Al	0	-2.84	3.39	0.84	1.95	0.98
Ga	0	-2.63	2.81	0.93	2.14	0.61
In	0	-2.49	2.52	0.99	2.44	0.65
Tl	0	-2.51	1.88	1.34	2.61	0.76

<sup>a</sup>Adsorption energies and adsorption structural properties for the favorable sites for the 11 adatoms are considered in this work. These include the binding energy ( $E_b$ ), adatom height ( $h$ ), and transferred charge from adatom using Bader charge analysis ( $\Delta e$ ). For reference, we include the experimental cohesive energy per atom of the bulk metal ( $E_c$ ) from ref 48 and the ratio of the adsorption energy to the bulk cohesive energy ( $|E_b|/E_c$ ).

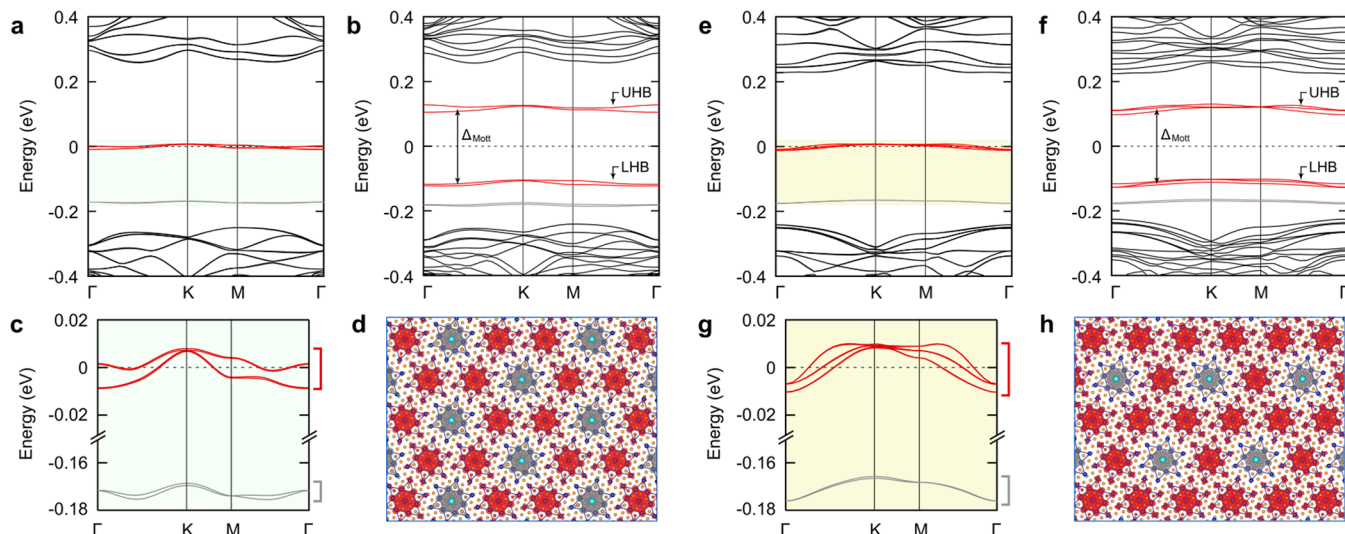


**Figure 3.** Half-filled Mott Dirac and kagome bands. Calculated band structure of a  $\text{TaS}_2$  monolayer with Na adatoms in a  $(\sqrt{3} \times \sqrt{3})R30^\circ$  superlattice with (a) a paramagnetic constraint and (b) the on-site Coulomb repulsion  $U = 1$  eV, respectively. (c) Enlargement of the band structure near the Fermi level in (a). (d) Spatial distribution of the metallic Dirac bands [marked with red in (c)] and fully occupied flat band at  $\sim -0.17$  eV [marked with gray in (c)]. Calculated band structure of a  $\text{TaS}_2$  monolayer with Na adatoms in a  $2 \times 2$  superlattice with (e) a paramagnetic constraint and (f) the on-site Coulomb repulsion  $U = 1$  eV, respectively. (g) Enlargement of the band structure near the Fermi level in (e). (h) Spatial distribution of the metallic kagome bands [marked with red in (g)] and a fully occupied flat band at  $\sim -0.17$  eV [marked with gray in (g)].

electron donated by Na. This band moves below the Fermi level by 0.17 eV (see the gray band in Figure 3a), leaving behind two bands at the Fermi level (marked with a red color in Figure 3a). These two bands form a Dirac band with a small bandwidth due to the hexagonal symmetry imposed. The fully occupied band moves farther down from the Fermi level without hybridizing with the Dirac bands, when the adatom potential is stronger going from Rb to Li. The narrow Dirac bands are still half-filled with its linear crossing at the K point (Figures 3a and 3c), consistent with the result of our TB model (Figure 1c). The bandwidth is only about  $\sim 20$  meV due to the localized character of the partially filled  $\text{Ta } d_z^2$  orbitals at the center of a DS and the huge size of the supercell. The direct hopping between these  $d$  orbitals in the hexagonal lattice is significantly limited, and the major hopping paths are achieved via  $p$  orbitals of S atoms.

It has been well established that the  $5d_z^2$  electron in the CDW unit cell of 1T- $\text{TaS}_2$  has a substantial on-site Coulomb interaction on the order of 1–2 eV to bring this CDW phase into a Mott insulating state. In order to describe the experimental Mott gap ( $\approx 250$  meV),<sup>17,23</sup> we have chosen an effective Hubbard  $U$  for Ta  $5d$  is 1 eV in the DFT+U calculation.<sup>38</sup> Similar to the case of the pristine triangular lattice, two sets of narrow bands, corresponding to the upper and lower Hubbard bands (UHB and LHB), are then produced with a Mott gap  $\Delta_{\text{Mott}} \sim 0.23$  eV, as shown in Figure 3b. Note, however, that both UHB and LHB bands have Dirac crossings (Figure S4a). The spatial charge distributions of Hubbard bands in the honeycomb lattice (Figure 3d) show that the electrons from the bare DSs are almost intact with their partially filled band localized at the center of DS.

Similarly, a kagome lattice can be produced by forming a  $2 \times 2$  superlattice with periodically adsorbed Na adatoms with lower coverage. Figures 3e and 3f show the band structures and charge density distributions in the kagome superlattice. There are three extremely narrow bands originating from three bare

DSs at the Fermi level and one fully occupied band from the Na-adsorbed DS around  $-0.17$  eV (Figures 3e and 3g). The three upper bands compose a set of “kagome bands”, where two Dirac bands have a Dirac point at K and have a quadratic touching at  $\Gamma$  with an inherently flat band. Since the bandwidth in the CDW  $\text{TaS}_2$  is already quite small,  $\sim 20$  meV, all the kagome bands are within this energy scale. When the effective  $U$  is included, the kagome bands are split into two sets with a Mott gap of  $\sim 0.23$  eV. The 2D mapping of electron charge densities sampled in the energy range of the kagome bands is displayed in Figure 3h. It is clear that the kagome pattern of local charge density exists as expected.

We further investigate the topology of these flat bands in both superlattices. The Kane-Mele model for a hexagonal lattice<sup>49</sup> or a kagome lattice model<sup>50</sup> yields a quantum spin Hall phase with gapless helical edge states when the spin-orbit coupling (SOC) is turned on. Considering SOC in the paramagnetic DFT calculation, one can see a tiny SOC gap at the K point for Dirac and kagome bands. The SOC gap at the K point is on the order of  $\sim 0.1$  meV. The topological invariant  $Z_2$  number has been calculated by checking the Wannier charge center evolution of occupied bands (Figure S5), which clearly indicates an odd number of crossings via the pumping parameter, a hallmark of nontrivial topology of  $Z_2 = 1$ . The nontrivial order can also be manifested by the presence of helical edge states (Figure 4). Although there is no global gap due to the characteristics of the present narrow bands, the 1D helical Dirac states of the zigzag edge can be confirmed at a specific  $k$  point,  $\Gamma$  or X point, for hexagonal or Kagome superlattices, respectively, as shown in the figure. Interestingly, in the case of the kagome lattice, two Dirac states appear because the topological gap exists both at the Dirac point and the parabolic touching point at  $\Gamma$ , respectively.<sup>51</sup> It is worth noting that increasing  $U$  does not break any symmetry as the system remains in the paramagnetic state. These results represent the correlated topological lattices can be described by a Kane-Mele Hubbard<sup>52</sup> or kagome-Hubbard model<sup>53–55</sup>

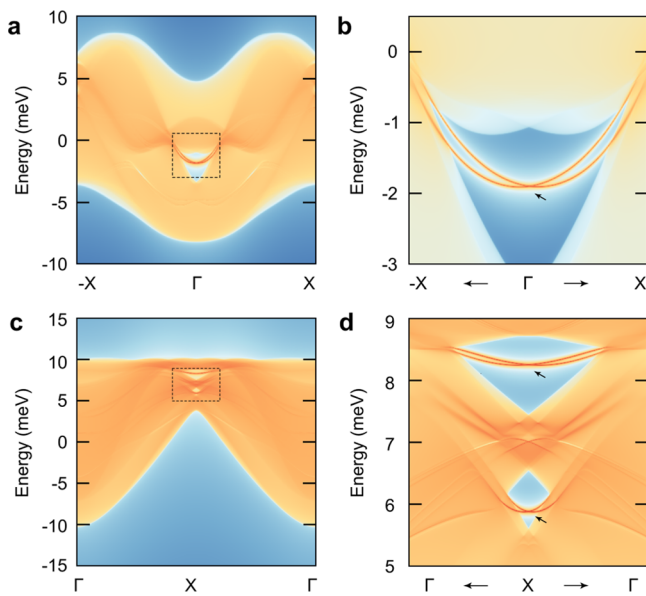


**Figure 4.** Helical edge states in Na-adsorbed 1T-TaS<sub>2</sub> in the paramagnetic phase. (a) Calculated edge states of  $\sqrt{3} \times \sqrt{3}$  Na-patterned TaS<sub>2</sub> with a zigzag boundary. (b) Enlarged image of the area indicated by a dashed square in (a). (c) Calculated edge state of  $2 \times 2$  Na-patterned TaS<sub>2</sub> with a zigzag boundary. (d) Enlarged image of the area indicated by a dashed square in (c).

(Figure S6). We note that the possible magnetic orderings in a honeycomb or kagome lattice are missing in the present work due to the extremely low magnetic ordering temperature [ $\sim O(mK)$ ].<sup>17</sup> Using a simple analogy, the system may become a Chern insulator for 1/4 and 3/4 fillings in a ferromagnetic ordering and a trivial one in an antiferromagnetic case (Figure S4). In addition, the Mott insulating nature of the present system is more clearly reproduced by DMFT calculation (Figure S7).

## ■ 2/3- OR 3/4-FILLED MOTT INSULATOR: MG DECORATED TAS<sub>2</sub> SYSTEM

As mentioned above, the charge state of the alkaline-earth metal on TaS<sub>2</sub> is +2, so two electrons from the alkaline-earth metal are transferred to the TaS<sub>2</sub> surface. However, as shown in the Na case, the maximum number of electrons that can be received per adsorbed DS is one. Therefore, an extra electron from the alkaline-earth metal must be transferred to another nearby DS without the adsorbed metal atom. This offers an opportunity to tune and control the filling of flat Dirac and kagome bands. On the other hand, from the adsorption energies and geometries, except for Mg, the alkaline-earth metals prefer the off-center site. This adsorption geometry breaks the symmetry of overall DSs in hexagonal or kagome lattices. Consequently, one may expect quite different features of the flat bands, generated by Ca and Sr adatoms, from what was predicted by the TB model. Therefore, below we will focus only on the band structures of hexagonal and kagome lattices with adsorption of the Mg adatom sitting in the highly symmetric site (center of the DS).

Figures 5a-5c show the calculated band structures of the hexagonal lattice with Mg adatoms in a  $\sqrt{3} \times \sqrt{3}$  supercell. As expected and as in the case of alkali metal adsorption, one electron from Mg fully occupies the narrow band at the adsorbed site, which is moved down to  $\sim -0.5$  eV below the bulk valence band (not shown in Figure 5a). The remaining electron is shared by two bare DS sites within a  $\sqrt{3} \times \sqrt{3}$  supercell. The charge density difference induced by the adsorption ( $\Delta\rho = \rho_{(Mg/TaS_2)} - \rho_{(TaS_2)} - \rho_{(Mg)}$ ) shows this clearly (Figure 5d). The two 3s valence electrons of Mg adatom are almost completely transferred to the substrate with one electron localized highly within a single DS and the other distributed equally in the adjacent two DSs constituting the hexagonal lattice. Consequently, the Dirac bands originating from these bare DS sites deviate from a half filling to an overall 3/4 filling (Figure 5c). In addition, we find that the local interaction of a Mg adatom with the TaS<sub>2</sub> surface is stronger

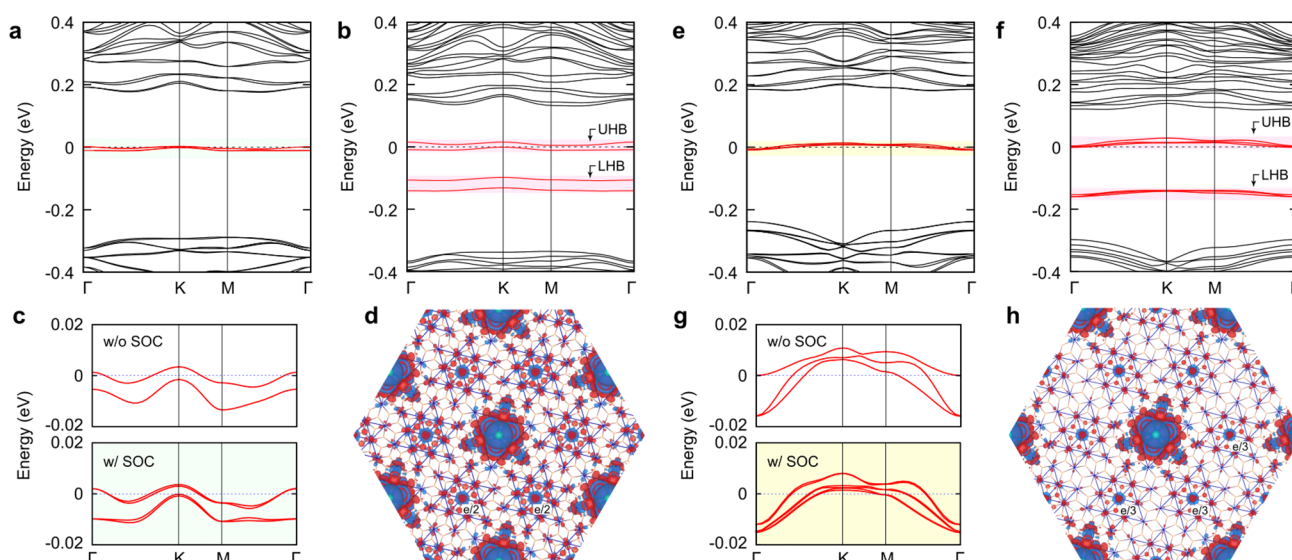


**Figure 5.** Fractional band filling of Mott Dirac and kagome bands. Calculated band structure of a TaS<sub>2</sub> monolayer with Mg adatoms in a  $(\sqrt{3} \times \sqrt{3})R30^\circ$  superlattice with (a) a paramagnetic constraint and (b) the on-site Coulomb repulsion  $U = 1$  eV, respectively. (c) Enlarged view of band structure without and with SOC near the Fermi level in (a). (d) Charge transfer from Mg adatoms. Red and blue colors represent accumulation and depletion of electron density, respectively. The plotted iso-level is  $\pm 3 \times 10^{-4}$  e/Å<sup>3</sup>. (e)-(h) Same as (a)-(d) for the  $2 \times 2$  TaS<sub>2</sub> superlattice.

than the alkali adatoms, which breaks the AB sublattice symmetry of the hexagonal lattice (Figure S1). As a result, a finite trivial gap of  $\sim 4$  meV appears at the K point in the Dirac band due to inversion asymmetry irrespective of SOC (Figure 5c). Including the effective on-site Coulomb energy  $U = 1$  eV opens a Mott gap of  $\sim 180$  meV (Figure 5b). It is worth noting that the Mott gap is smaller than the Na case because the overall bandwidth is increased two times. At the same time, the trivial gap at K is increased to 32 meV (17 meV) for LHB (UHB) by the  $U$  correction. Of course, the 3/4-filling condition is preserved leading to a 3/4-filled Mott system with the Fermi level within UHB.

We perform similar calculations for the kagome lattice patterned by Mg adatoms. Figures 5e and 5f show the band structures obtained with a paramagnetic constraint and in DFT + $U$  approximation, respectively. Similar to the hexagonal lattice, one electron from a Mg adatom fully occupies the narrow band from the adsorbed DS site, and the remaining electron is equally distributed to three adjacent bare DS sites, namely,  $e/3$  on each bare site. In the charge density difference plot (Figure 5h), it can be seen that the charge density distribution is consistent with the 2/3 band filling. Some charge accumulation can be seen at the center of the three bare DS sites adjacent to the Mg adsorbed DS. Accordingly, the kagome bands originating from the bare DS sites are occupied uniformly by the excessive electron, leading to an overall 2/3 band filling (Figures 5e and 5g). With the inclusion of the Hubbard interaction, the fully occupied bands around  $-0.16$  eV form the lower Hubbard kagome bands (Figure 5f) and the upper Hubbard kagome bands are 16.67% occupied (Figure 5g).

As shown above, we get doped Mott insulators with hexagonal and kagome symmetry by the adsorption of alkaline-earth metals on 1T-TaS<sub>2</sub>. An important consequence of the doped Mott insulator is superconductivity. Recently Phillips et al.<sup>56</sup> demonstrated an analog of the Cooper instability for a correlated electron model of a doped Mott insulator. They showed that the metallic phases in the doped Mott insulator exhibit non-Fermi liquid character with a superconducting instability. This suggests that the 2/3- or 3/4-filled TaS<sub>2</sub> Mott system may similarly realize the superconducting phase. By approximating the bandwidth  $W$  ( $\sim 20$  meV) as in the paramagnetic TaS<sub>2</sub> and the effective electron-electron interaction  $U_{\text{eff}}$  (180–230 meV) as the Mott gap of the doped TaS<sub>2</sub> system, we estimate a range of  $U_{\text{eff}}/W \sim 9$ –11.5, which is in line with the other theoretical calculations for TaS<sub>2</sub> ( $U_{\text{eff}}/W \sim 2.6$ –9.3). Given that  $U_{\text{eff}}/W \approx 9$ , when the Hubbard bands cross the chemical potential, the doped TaS<sub>2</sub> Mott system lies in a regime very close to the superconducting phase.<sup>56</sup> This is an exciting possibility to be checked with future experiments.

We have proposed a practical approach to creating correlated topological electronic states in the 1T-TaS<sub>2</sub> flat-band system. The resulting strongly correlated topological lattices including a kagome lattice can be deliberately tuned by the supercell periodicity and the selective deposition of metal adatoms onto 1T-TaS<sub>2</sub>. Our study not only reveals the interplay between the flatness of electronic bands and band topology but also shows a route to the emergence of unconventional superconductivity in a doped Mott system. The physical mechanism underlying the proposed lattice manipulation approach by adsorbate superstructures is general and can be extended to various 2D materials with narrow

bands as well as to moiré superstructures. In addition, the high tenability associated with adatom degrees of freedom can be especially appealing to future experimental studies for achieving charge doping of flat bands and strong coupling with magnetic impurity.

## ■ ASSOCIATED CONTENT

### SI Supporting Information

The Supporting Information is available free of charge at <https://pubs.acs.org/doi/10.1021/acs.nanolett.2c02866>.

Computational methods, atomic displacement of Ta atoms in 1T-TaS<sub>2</sub>, band structures of metal-decorated TaS<sub>2</sub> in  $(\sqrt{3} \times \sqrt{3})R30^\circ$  and  $2 \times 2$  superlattices, correlation effect in DFT+ $U$  and DMFT approaches, topological character for Na adsorbed TaS<sub>2</sub>, and tight binding Hamiltonian of metal adsorbed 1T-TaS<sub>2</sub> (PDF)

## ■ AUTHOR INFORMATION

### Corresponding Authors

Kyung-Hwan Jin – Center for Artificial Low Dimensional Electronic Systems, Institute for Basic Science (IBS), Pohang 37673, Republic of Korea; [orcid.org/0000-0002-5116-9987](https://orcid.org/0000-0002-5116-9987); Email: [khwanjin@gmail.com](mailto:khwanjin@gmail.com)

Han Woong Yeom – Center for Artificial Low Dimensional Electronic Systems, Institute for Basic Science (IBS), Pohang 37673, Republic of Korea; Department of Physics, Pohang University of Science and Technology, Pohang 37673, Republic of Korea; [orcid.org/0000-0002-8538-8993](https://orcid.org/0000-0002-8538-8993); Email: [yeom@postech.ac.kr](mailto:yeom@postech.ac.kr)

### Authors

Dongheon Lee – Center for Artificial Low Dimensional Electronic Systems, Institute for Basic Science (IBS), Pohang 37673, Republic of Korea

Feng Liu – Department of Materials Science and Engineering, University of Utah, Salt Lake City, Utah 84112, United States; [orcid.org/0000-0002-3701-8058](https://orcid.org/0000-0002-3701-8058)

Complete contact information is available at: <https://pubs.acs.org/10.1021/acs.nanolett.2c02866>

### Author Contributions

K.H.J. and H.W.Y. conceived the research idea and plan. D.L. and K.H.J. performed the first-principles and model calculations. All authors contributed to the interpretation, the discussion of the results, and the manuscript.

### Notes

The authors declare no competing financial interest.

## ■ ACKNOWLEDGMENTS

This work was supported by the Institute for Basic Science (Grant No. IBS-R014-D1). D.L. and K.-H.J. are supported by the Institute for Basic Science (Grant No. IBS-R014-Y1). F.L. acknowledges the support from the US-DOE (Grant No. DE-FG02-04ER46148).

## ■ REFERENCES

- (1) Polini, M.; Guinea, F.; Lewenstein, M.; Manoharan, H. C.; Pellegrini, V. Artificial honeycomb lattices for electrons, atoms and photons. *Nat. Nanotechnol.* **2013**, *8* (9), 625–633.
- (2) Gomes, K. K.; Mar, W.; Ko, W.; Guinea, F.; Manoharan, H. C. Designer Dirac fermions and topological phases in molecular graphene. *Nature* **2012**, *483* (7389), 306–310.

- (3) Park, C.-H.; Louie, S. G. Making Massless Dirac Fermions from a Patterned Two-Dimensional Electron Gas. *Nano Lett.* **2009**, *9* (5), 1793–1797.
- (4) Gibertini, M.; Singha, A.; Pellegrini, V.; Polini, M.; Vignale, G.; Pinczuk, A.; Pfeiffer, L. N.; West, K. W. Engineering artificial graphene in a two-dimensional electron gas. *Phys. Rev. B* **2009**, *79* (24), 241406.
- (5) Slot, M. R.; Gardenier, T. S.; Jacobse, P. H.; van Miert, G. C. P.; Kempkes, S. N.; Zevenhuizen, S. J. M.; Smith, C. M.; Vanmaekelbergh, D.; Swart, I. Experimental realization and characterization of an electronic Lieb lattice. *Nat. Phys.* **2017**, *13* (7), 672–676.
- (6) Paavilainen, S.; Ropo, M.; Nieminen, J.; Akola, J.; Räsänen, E. Coexisting Honeycomb and Kagome Characteristics in the Electronic Band Structure of Molecular Graphene. *Nano Lett.* **2016**, *16* (6), 3519–3523.
- (7) Wunsch, B.; Guinea, F.; Sols, F. Dirac-point engineering and topological phase transitions in honeycomb optical lattices. *New J. Phys.* **2008**, *10* (10), 103027.
- (8) Soltan-Panahi, P.; Struck, J.; Hauke, P.; Bick, A.; Plenkers, W.; Meineke, G.; Becker, C.; Windpassinger, P.; Lewenstein, M.; Sengstock, K. Multi-component quantum gases in spin-dependent hexagonal lattices. *Nat. Phys.* **2011**, *7* (5), 434–440.
- (9) Tarruell, L.; Greif, D.; Uehlinger, T.; Jotzu, G.; Esslinger, T. Creating, moving and merging Dirac points with a Fermi gas in a tunable honeycomb lattice. *Nature* **2012**, *483* (7389), 302–305.
- (10) Haldane, F. D. M.; Raghu, S. Possible Realization of Directional Optical Waveguides in Photonic Crystals with Broken Time-Reversal Symmetry. *Phys. Rev. Lett.* **2008**, *100* (1), 013904.
- (11) Khanikaev, A. B.; Hossein Mousavi, S.; Tse, W.-K.; Kargarian, M.; MacDonald, A. H.; Shvets, G. Photonic topological insulators. *Nat. Mater.* **2013**, *12* (3), 233–239.
- (12) Ni, X.; Weiner, M.; Alù, A.; Khanikaev, A. B. Observation of higher-order topological acoustic states protected by generalized chiral symmetry. *Nat. Mater.* **2019**, *18* (2), 113–120.
- (13) Zhou, M.; Ming, W.; Liu, Z.; Wang, Z.; Li, P.; Liu, F. Epitaxial growth of large-gap quantum spin Hall insulator on semiconductor surface. *Proc. Natl. Acad. Sci. U.S.A.* **2014**, *111* (40), 14378–14381.
- (14) Zhou, M.; Ming, W.; Liu, Z.; Wang, Z.; Yao, Y.; Liu, F. Formation of quantum spin Hall state on Si surface and energy gap scaling with strength of spin orbit coupling. *Sci. Rep.* **2015**, *4* (1), 7102.
- (15) Jin, K.-H.; Jhi, S.-H. Quantum anomalous Hall and quantum spin-Hall phases in flattened Bi and Sb bilayers. *Sci. Rep.* **2015**, *5* (1), 8426.
- (16) Reis, F.; Li, G.; Dudy, L.; Bauernfeind, M.; Glass, S.; Hanke, W.; Thomale, R.; Schäfer, J.; Claessen, R. Bismuthene on a SiC substrate: A candidate for a high-temperature quantum spin Hall material. *Science* **2017**, *357* (6348), 287–290.
- (17) Lee, J.; Jin, K.-H.; Catuneanu, A.; Go, A.; Jung, J.; Won, C.; Cheong, S.-W.; Kim, J.; Liu, F.; Kee, H.-Y.; Yeom, H. W. Honeycomb-Lattice Mott Insulator on Tantalum Disulphide. *Phys. Rev. Lett.* **2020**, *125* (9), 096403.
- (18) Fazekas, P.; Tosatti, E. Electrical, structural and magnetic properties of pure and doped 1T-TaS<sub>2</sub>. *Philos. Mag. Part B* **1979**, *39* (3), 229–244.
- (19) Perfetti, L.; Loukakos, P. A.; Lisowski, M.; Bovensiepen, U.; Berger, H.; Biermann, S.; Cornaglia, P. S.; Georges, A.; Wolf, M. Time Evolution of the Electronic Structure of 1T-TaS<sub>2</sub> through the Insulator-Metal Transition. *Phys. Rev. Lett.* **2006**, *97* (6), 067402.
- (20) Darancet, P.; Millis, A. J.; Marianetti, C. A. Three-dimensional metallic and two-dimensional insulating behavior in octahedral tantalum dichalcogenides. *Phys. Rev. B* **2014**, *90* (4), 045134.
- (21) Ritschel, T.; Trinckauf, J.; Koepernik, K.; Büchner, B.; Zimmermann, M. v.; Berger, H.; Joe, Y. I.; Abbamonte, P.; Geck, J. Orbital textures and charge density waves in transition metal dichalcogenides. *Nat. Phys.* **2015**, *11* (4), 328–331.
- (22) Cho, D.; Cheon, S.; Kim, K.-S.; Lee, S.-H.; Cho, Y.-H.; Cheong, S.-W.; Yeom, H. W. Nanoscale manipulation of the Mott insulating state coupled to charge order in 1T-TaS<sub>2</sub>. *Nat. Commun.* **2016**, *7* (1), 10453.
- (23) Butler, C. J.; Yoshida, M.; Hanaguri, T.; Iwasa, Y. Mottness versus unit-cell doubling as the driver of the insulating state in 1T-TaS<sub>2</sub>. *Nat. Commun.* **2020**, *11* (1), 2477.
- (24) Lee, J. M.; Geng, C.; Park, J. W.; Oshikawa, M.; Lee, S.-S.; Yeom, H. W.; Cho, G. Y. Stable Flatbands, Topology, and Superconductivity of Magic Honeycomb Networks. *Phys. Rev. Lett.* **2020**, *124* (13), 137002.
- (25) Pizarro, J. M.; Adler, S.; Zantout, K.; Mertz, T.; Barone, P.; Valentí, R.; Sangiovanni, G.; Wehling, T. O. Deconfinement of Mott localized electrons into topological and spin-orbit-coupled Dirac fermions. *npj Quantum Mater.* **2020**, *5* (1), 79.
- (26) Nayak, A. K.; Steinbok, A.; Roet, Y.; Koo, J.; Margalit, G.; Feldman, I.; Almoalem, A.; Kanigel, A.; Fiete, G. A.; Yan, B.; Oreg, Y.; Avraham, N.; Beidenkopf, H. Evidence of topological boundary modes with topological nodal-point superconductivity. *Nat. Phys.* **2021**, *17* (12), 1413–1419.
- (27) Law, K. T.; Lee, P. A. 1T-TaS<sub>2</sub> as a quantum spin liquid. *Proc. Natl. Acad. Sci. U.S.A.* **2017**, *114* (27), 6996–7000.
- (28) Sipos, B.; Kusmartseva, A. F.; Akrap, A.; Berger, H.; Forró, L.; Tuttiš, E. From Mott state to superconductivity in 1T-TaS<sub>2</sub>. *Nat. Mater.* **2008**, *7* (12), 960–965.
- (29) Ang, R.; Tanaka, Y.; Ieki, E.; Nakayama, K.; Sato, T.; Li, L. J.; Lu, W. J.; Sun, Y. P.; Takahashi, T. Real-Space Coexistence of the Melted Mott State and Superconductivity in Fe-Substituted 1T-TaS<sub>2</sub>. *Phys. Rev. Lett.* **2012**, *109* (17), 176403.
- (30) Mañas-Valero, S.; Huddart, B. M.; Lancaster, T.; Coronado, E.; Pratt, F. L. Quantum phases and spin liquid properties of 1T-TaS<sub>2</sub>. *npj Quantum Mater.* **2021**, *6* (1), 69.
- (31) Zhu, X.-Y.; Wang, S.; Jia, Z.-Y.; Zhu, L.; Li, Q.-Y.; Zhao, W.-M.; Xue, C.-L.; Xu, Y.-J.; Ma, Z.; Wen, J.; Yu, S.-L.; Li, J.-X.; Li, S.-C. Realization of a Metallic State in 1T-TaS<sub>2</sub> with Persisting Long-Range Order of a Charge Density Wave. *Phys. Rev. Lett.* **2019**, *123* (20), 206405.
- (32) Lee, J.; Jin, K.-H.; Yeom, H. W. Distinguishing a Mott Insulator from a Trivial Insulator with Atomic Adsorbates. *Phys. Rev. Lett.* **2021**, *126* (19), 196405.
- (33) Yao, Q.; Park, J. W.; Oh, E.; Yeom, H. W. Engineering Domain Wall Electronic States in Strongly Correlated van der Waals Material of 1T-TaS<sub>2</sub>. *Nano Lett.* **2021**, *21* (22), 9699–9705.
- (34) He, W.-Y.; Xu, X. Y.; Chen, G.; Law, K. T.; Lee, P. A. Spinon Fermi Surface in a Cluster Mott Insulator Model on a Triangular Lattice and Possible Application to 1T-TaS<sub>2</sub>. *Phys. Rev. Lett.* **2018**, *121* (4), 046401.
- (35) Liu, Z.; Liu, F.; Wu, Y.-S. Exotic electronic states in the world of flat bands: From theory to material. *Chin. Phys. B* **2014**, *23* (7), 077308.
- (36) Kresse, G.; Furthmüller, J. Efficient iterative schemes for ab initio total-energy calculations using a plane-wave basis set. *Phys. Rev. B* **1996**, *54* (16), 11169–11186.
- (37) Perdew, J. P.; Burke, K.; Ernzerhof, M. Generalized Gradient Approximation Made Simple. *Phys. Rev. Lett.* **1996**, *77* (18), 3865–3868.
- (38) Dudarev, S. L.; Botton, G. A.; Savrasov, S. Y.; Humphreys, C. J.; Sutton, A. P. Electron-energy-loss spectra and the structural stability of nickel oxide: An LSDA+U study. *Phys. Rev. B* **1998**, *57* (3), 1505–1509.
- (39) Mostofi, A. A.; Yates, J. R.; Lee, Y.-S.; Souza, I.; Vanderbilt, D.; Marzari, N. wannier90: A tool for obtaining maximally-localised Wannier functions. *Comput. Phys. Commun.* **2008**, *178* (9), 685–699.
- (40) Sancho, M. P. L.; Sancho, J. M. L.; Rubio, J. Quick iterative scheme for the calculation of transfer matrices: application to Mo (100). *J. Phys. F* **1984**, *14* (5), 1205–1215.
- (41) Wu, Q.; Zhang, S.; Song, H.-F.; Troyer, M.; Soluyanov, A. A. WannierTools: An open-source software package for novel topological materials. *Comput. Phys. Commun.* **2018**, *224*, 405–416.

- (42) Li, L. J.; Lu, W. J.; Zhu, X. D.; Ling, L. S.; Qu, Z.; Sun, Y. P. Fe-doping-induced superconductivity in the charge-density-wave system 1T-TaS<sub>2</sub>. *EPL* **2012**, *97* (6), 67005.
- (43) Li, L. J.; Lu, W. J.; Liu, Y.; Qu, Z.; Ling, L. S.; Sun, Y. P. Influence of defects on charge-density-wave and superconductivity in 1T-TaS<sub>2</sub> and 2H-TaS<sub>2</sub> systems. *Physica C* **2013**, *492*, 64–67.
- (44) Yu, Y.; Yang, F.; Lu, X. F.; Yan, Y. J.; Cho, Y.-H.; Ma, L.; Niu, X.; Kim, S.; Son, Y.-W.; Feng, D.; Li, S.; Cheong, S.-W.; Chen, X. H.; Zhang, Y. Gate-tunable phase transitions in thin flakes of 1T-TaS<sub>2</sub>. *Nat. Nanotechnol.* **2015**, *10* (3), 270–276.
- (45) Zhang, W.; Gao, J.; Cheng, L.; Bu, K.; Wu, Z.; Fei, Y.; Zheng, Y.; Wang, L.; Li, F.; Luo, X.; Liu, Z.; Sun, Y.; Yin, Y. Visualizing the evolution from Mott insulator to Anderson insulator in Ti-doped 1T-TaS<sub>2</sub>. *npj Quantum Mater.* **2022**, *7* (1), 8.
- (46) Tang, W.; Sanville, E.; Henkelman, G. A grid-based Bader analysis algorithm without lattice bias. *J. Phys.: Condens. Matter.* **2009**, *21* (8), 084204.
- (47) Chan, K. T.; Neaton, J. B.; Cohen, M. L. First-principles study of metal adatom adsorption on graphene. *Phys. Rev. B* **2008**, *77* (23), 235430.
- (48) Kittel, C. *Introduction to Solid State Physics*, 8th ed.; John Wiley & Sons: 2004.
- (49) Kane, C. L.; Mele, E. J. Quantum Spin Hall Effect in Graphene. *Phys. Rev. Lett.* **2005**, *95* (22), 226801.
- (50) Wang, Z.; Zhang, P. Quantum spin Hall effect and spin-charge separation in a kagomé lattice. *New J. Phys.* **2010**, *12* (4), 043055.
- (51) Guo, H. M.; Franz, M. Topological insulator on the kagomé lattice. *Phys. Rev. B* **2009**, *80* (11), 113102.
- (52) Hohenadler, M.; Meng, Z. Y.; Lang, T. C.; Wessel, S.; Muramatsu, A.; Assaad, F. F. Quantum phase transitions in the Kane-Mele-Hubbard model. *Phys. Rev. B* **2012**, *85* (11), 115132.
- (53) Mielke, A. Exact ground states for the Hubbard model on the Kagome lattice. *J. Phys. A* **1992**, *25* (16), 4335–4345.
- (54) Ohashi, T.; Kawakami, N.; Tsunetsugu, H. Mott Transition in Kagome Lattice Hubbard Model. *Phys. Rev. Lett.* **2006**, *97* (6), 066401.
- (55) Kim, S. K.; Zang, J. U(1) symmetry of the spin-orbit coupled Hubbard model on the kagomé lattice. *Phys. Rev. B* **2015**, *92* (20), 205106.
- (56) Phillips, P. W.; Yeo, L.; Huang, E. W. Exact theory for superconductivity in a doped Mott insulator. *Nat. Phys.* **2020**, *16* (12), 1175–1180.

## □ Recommended by ACS

### Multivalley Superconductivity in Monolayer Transition Metal Dichalcogenides

Dongdong Ding, Jianming Lu, *et al.*  
SEPTEMBER 29, 2022  
NANO LETTERS

READ ▶

### Fourfold Symmetric Superconductivity in Spinel Oxide LiTi<sub>2</sub>O<sub>4</sub>(001) Thin Films

Huanyi Xue, Wei Li, *et al.*  
NOVEMBER 04, 2022  
ACS NANO

READ ▶

### Superconductivity on Edge: Evidence of a One-Dimensional Superconducting Channel at the Edges of Single-Layer FeTeSe Antiferromagnetic Nanoribbons

Zhuozhi Ge, Lian Li, *et al.*  
MAY 04, 2020  
ACS NANO

READ ▶

### Mitrofanovite Pt<sub>3</sub>Te<sub>4</sub>: A Topological Metal with Termination-Dependent Surface Band Structure and Strong Spin Polarization

Jun Fujii, Antonio Politano, *et al.*  
SEPTEMBER 02, 2021  
ACS NANO

READ ▶

Get More Suggestions >